

Digital twins of the mooring line tension for floating offshore wind turbines to improve monitoring, lifespan, and safety

Walker, Jake; Coraddu, Andrea; Collu, Maurizio; Oneto, Luca

DOI

[10.1007/s40722-021-00213-y](https://doi.org/10.1007/s40722-021-00213-y)

Publication date

2021

Document Version

Final published version

Published in

Journal of Ocean Engineering and Marine Energy

Citation (APA)

Walker, J., Coraddu, A., Collu, M., & Oneto, L. (2021). Digital twins of the mooring line tension for floating offshore wind turbines to improve monitoring, lifespan, and safety. *Journal of Ocean Engineering and Marine Energy*, 8(1). <https://doi.org/10.1007/s40722-021-00213-y>

Important note

To cite this publication, please use the final published version (if applicable). Please check the document version above.

Copyright

Other than for strictly personal use, it is not permitted to download, forward or distribute the text or part of it, without the consent of the author(s) and/or copyright holder(s), unless the work is under an open content license such as Creative Commons.

Takedown policy

Please contact us and provide details if you believe this document breaches copyrights. We will remove access to the work immediately and investigate your claim.



Digital twins of the mooring line tension for floating offshore wind turbines to improve monitoring, lifespan, and safety

Jake Walker¹ · Andrea Coraddu^{1,3} · Maurizio Collu¹ · Luca Oneto²

Received: 14 July 2021 / Accepted: 3 September 2021 / Published online: 24 September 2021
© The Author(s) 2021

Abstract

The number of installed floating offshore wind turbines (FOWTs) has doubled since 2017, quadrupling the total installed capacity, and is expected to increase significantly over the next decade. Consequently, there is a growing consideration towards the main challenges for FOWT projects: monitoring the system's integrity, extending the lifespan of the components, and maintaining FOWTs safely at scale. Effectively and efficiently addressing these challenges would unlock the wide-scale deployment of FOWTs. In this work, we focus on one of the most critical components of the FOWTs, the Mooring Lines (MoLs), which are responsible for fixing the structure to the seabed. The primary mechanical failure mechanisms in MoLs are extreme load and fatigue, both of which are functions of the axial tension. An effective solution to detect long-term drifts in the mechanical response of the MoLs is to develop a Digital Twin (DT) able to accurately predict the behaviour of the healthy system to compare with the actual one. Moreover, we will develop another DT able to accurately predict the near future axial tension as an effective tool to improve the lifespan of the MoLs and the safety of FOWT maintenance operations. In fact, by changing the FOWT operational settings, according to the DT prediction, operators can increase the lifespan of the MoLs by reducing the stress and, additionally, in the case where FOWT operational maintenance is in progress, the prediction from the DT can serve as early safety warning to operators. Authors will leverage operational data collected from the world's first commercial floating-wind farm [the Hywind Pilot Park (<https://www.equinor.com/en/what-we-do/floating-wind/hywind-scotland.html>)] in 2018, to investigate the effectiveness of DTs for the prediction of the MoL axial tension for the two scenarios depicted above. The DTs will be developed using state-of-the-art data-driven methods, and results based on real operational data will support our proposal.

Keywords Floating offshore wind turbines · Mooring lines · Axial tension · Digital twins · Data-driven models

1 Introduction

Floating wind is one of the fastest-growing sectors within the Offshore Renewable Energy Industry and internationally recognised as one of the most promising renewable energy sources to satisfy a significant proportion of global energy demands (Carbon Trust 2015). The ability to economically deploy floating offshore wind turbines (FOWTs) in deepwater areas, that were previously unfeasible for development using fixed-bottom turbines, is one of the fundamental driving forces behind the success of floating wind (Carbon Trust 2018). In fact, deepwater areas are often characterised by higher average wind speeds and consequently an higher average capacity factors that could improve the economic viability of offshore wind energy (Hannon et al. 2019). However, floating wind is still an emerging market, and only a limited number of pilots have been deployed, so there is still

✉ Andrea Coraddu
andrea.coraddu@strath.ac.uk; a.coraddu@tudelft.nl

Jake Walker
jake.walker@strath.ac.uk

Maurizio Collu
maurizio.collu@strath.ac.uk

Luca Oneto
luca.oneto@unige.it

¹ NAOME, University of Strathclyde, 16 Richmond St, Glasgow G1 1XQ, UK

² DIBRIS, University of Genova, Via Opera Pia 13, 16145 Genoa, Italy

³ Faculty of Mechanical, Maritime and Materials Engineering, Delft University of Technology, Mekelweg 2, 2628 CD Delft, The Netherlands

a significant amount work required to address the unique aspects to floating wind: monitoring the system's integrity, extending the lifespan of the components, and maintaining FOWTs safely at scale (Carbon Trust 2015, 2018, 2020). Nevertheless, due to the success of Pilot FOWTs around the world, the industry is now focused on addressing these remaining challenges before deploying FOWTs at scale in deepwater (Carbon Trust 2020). In particular, the use, monitoring, and maintenance of the station-keeping devices (i.e., the Mooring Lines—MoLs) devoted to anchor the FOWT structure in place pose some of the most prominent challenges to overcome (Carbon Trust 2020).

Experience from the Oil&Gas industry indicates that the demanding environmental conditions such as the corrosive salt water and forceful waves, combined with the isolation of the deployment sites, are particularly damaging to the MoLs and may pose issues for checking and maintaining the integrity of FOWTs (Butterfield et al. 2007). In addition, unlike floating production storage and offloading (FPSO) vessels, where there are typically between 12 and 24 MoLs, economic drivers within the renewables sector tend to produce designs with no redundancy (Fugro 2020). For this reason, each MoL is critical to the FOWT structure, and failure is catastrophic (Ma et al. 2020). Nevertheless, the extreme conditions in which MoLs operate call for regular inspections to prevent disastrous failures and downtime. Inspections are usually performed in two ways: (1) close visual inspection by divers and (2) through remotely operated vehicles (ROVs) (Brown et al. 2005). When considering (1), diver inspections are not favoured due to the risk related to operating in deep water and human bias (Angulo et al. 2017). Similarly, with (2), ROVs are employed with limited success, since they need to be re-calibrated between successive measurements, and such may present errors in transmitting their positioning, affecting the localisation of damage (ABSG Consulting 2015). Moreover, both options remain uneconomical (ABSG Consulting 2015). For these reasons, within the Oil and Gas industry, alternative strategies for monitoring MoLs integrity are actually employed, like using load cell to detect rapid failure by extreme load (Lu 2016) or using GPS-based devices (e.g., LifeLine JIP (Marin LifeLine 2021)) to detect an unusual excursion caused by the loss of a single mooring (Marin LifeLine 2021).

Regarding FOWT failures and maintenance activities, since this industry is in its infancy, there are very little publicly available data describing the expected failure rates of FOWTs or the required maintenance schedules (Santos et al. 2016). According to (Röckmann et al. 2017) for a fixed-bottom offshore wind farm with 200 turbines, it may be necessary to perform up to 3000 maintenance visits per year. Since the mechanics of FOWTs are similar to the fixed-bottom turbines, it is safe to consider Floating-Wind farms will require (at least) a similar number of maintenance vis-

its. With this in mind, the ability to schedule maintenance by forecasting the health status of FOWTs becomes fundamental to deploy FOWTs maintenance at scale (Ren et al. 2021). Similar considerations should also be made towards the safety of the maintenance operations. In fact, since a failure could be catastrophic (Ma et al. 2020), developing an early warning system able to predict a failure early enough to secure a safe working environment is essential to ensure the safety of maintenance operations.

To forecast MoL failures (short term) or health conditions (long term), it is required to develop computational models of the mooring systems. Contrarily to visual inspections, computational models can ensure an economic, reliable, and effective monitoring tools for the integrity of the MoLs (Angulo et al. 2017).

In the literature, it is possible to find a large body of work addressing MoL failures (Ma et al. 2013; Davidson and Ringwood 2017; Brown et al. 2005; Al-Solihat and Nahon 2018; Aranha and Pinto 2001; Bhinder et al. 2015; Borg et al. 2014; Hsu et al. 2014, 2015; Jin and Kim 2018; Qiao et al. 2020; Maroju et al. 2013; de Pina et al. 2013; Prislín and Maroju 2017; Jaiswal and Ruskin 2019; Li et al. 2018). The primary mechanical failure mechanisms in mooring systems are extreme load and fatigue, both of which are functions of the axial tension (Davidson and Ringwood 2017). By exploiting this relationship, it is possible to use the MoL axial tension as an indicator for the health status of the Mooring System. In addition, (Brown et al. 2005) acknowledge MoL failures are often focused at the top of the chain, as these are the points of highest tension and the most stressed locations. The works available in the literature can be grouped into two main families: Physical Models (PMs) and Data-Driven Models (DDMs). PMs and DDMs can be used to detect long-term drifts in the mechanical response of the MoLs by developing a Digital Twin (DT) able to accurately predict the behaviour of the healthy system to compare with the actual one. A DT is a specific type of model that embodies a precise digital copy of a physical system (Oneto et al. 2018). Consequently, DTs are an effective method of forecasting the future behaviour of a system after the DT has learned the behaviour from historical examples (Coraddu et al. 2021). Moreover, as an effective tool to improve the lifespan of the MoLs and safety of FOWT maintenance operations, it is possible to develop DTs to predict the near future axial tension.

Concerning the PMs, they are primarily based on the mechanistic knowledge of the MoLs behaviour. Borg et al. (2014) provided a good overview of the mooring dynamics PMs, ranging from simple, quick but approximate methods (linear force–displacement or force–displacement–velocity models), to the high fidelity, but computationally expensive methods (finite-element approach), comparing the main characteristics, as shown in Table 1.

Table 1 Mooring dynamics PMs, adapted from (Borg et al. 2014)

Capability	Linear F–D–V	Quasi static	Multibody	Finite element
Static (average) tension	✓	✓	✓	✓
Individual line tension		✓	✓	✓
Line-seabed interaction		✓	✓	✓
Line longitudinal stiffness		✓	✓	✓
Line bending stiffness			✓	✓
Line inertia/hydro-damping			✓	✓
Line torsional stiffness				✓

Focusing on failure modes, the linear model is not suitable, since it is valid only within a limited range of platform displacements (therefore not suitable for extreme loads), and by definition, it does not capture the non-linear dynamics of the tension and such, can under/overestimate the tension cycles. Moreover, it only models the total tension of all the mooring lines; therefore, no information about the tension in the single lines can be inferred (Cevasco et al. 2018). The quasi-static model is capable of modelling the single line tension and the non-linearity of the tension in the MoLs. It is considered suitable to estimate the global response motion of the platform, but may not be as accurate as a fully dynamic model (such as Multibody or Finite Elements) at predicting single line tension (Karimirad 2013). In particular, while at static level, a quasi-static model can be in very good agreement with multibody or finite-element models. However, when considering a stochastic load condition (e.g., random waves from a wave spectrum), the dynamic tension oscillation may be overestimated, since the inertia of the lines and, more importantly, the hydrodynamic viscous damping loads acting on the mooring lines are not captured (Hall et al. 2014). The multibody mooring model (also called the “lumped mass approach”) is able to capture the effects of the line inertial loads and the hydrodynamic viscous forces acting on the mooring lines, and it is also suitable to estimate the extreme and oscillatory tension loads at a preliminary design stage, since it is characterised by a sufficient accuracy but still within an acceptable computational cost (Cevasco et al. 2018). The finite-element method is suggested for very accurate analyses, but this is usually reserved for a limited set of load cases/simulations, typically at an advanced design stage, due to its substantially higher computational costs (Cevasco et al. 2018; Hall et al. 2014).

Instead, DDMs allow us to develop computationally aware real-time monitoring systems for MoLs by learning the input–output behaviour of a system from historical examples without any a-priori knowledge about the MoLs. DDMs require a single intensive learning phase (i.e., model construction) and benefit from a computationally inexpensive forward phase (i.e., model used as a predictor) (Coraddu

et al. 2020), making them well suited to develop DTs. Maroju et al. (2013); de Pina et al. (2013); Prislín and Maroju (2017); Jaiswal and Ruskin (2019) have all proposed using DDMs to monitor other marine energy systems (Floating platforms, FPSO vessels, etc.), and noted the potential for predictive models to reduce the cost of operational monitoring. In particular, de Pina et al. (2013) propose a DDM to approximate the MoL tension in place of a computationally expensive PM (specifically a Finite-Element Analysis) by use of a non-linear autoregressive exogenous model. This model could accurately simulate the tension response over a period of multiple hours; however, the algorithm was effective only in forecasting the tension in the short term (0.1s). Fatigue damage of MoLs has been investigated by (Li et al. 2018) using an Artificial Neural Network (ANN), where they observe the significant influence of the environmental conditions (waves, winds, and currents) on the tension bands. Additionally, (Hsu et al. 2015, 2017) demonstrate the potential benefits of using DDMs for FOWT MoLs when scaling health monitoring tools site-wide.

To the best of the authors’ knowledge, no one has yet developed DTs of the FOWT MoLs to detect long-term drifts in the mechanical response or to accurately predict the near future axial tension. Moreover, the previous literature on monitoring FOWTs has been focused only on synthetic data and scenarios. Developing strategies to address these problems and testing the solutions with real data could provide the necessary information to address the outlined challenges sufficiently. Specifically, the DT prediction could be used to change the FOWT operational settings to increase the lifespan of the MoLs by reducing the stress and, additionally, in the case where FOWT operational maintenance is in progress, serve as an early safety warning to operators.

For these reasons, to detect long-term drifts in the mechanical response of the MoLs, we will develop a DT able to accurately predict the behaviour of the healthy system to compare with the actual one. Moreover, as an effective tool to improve the lifespan of the MoLs and safety of FOWT maintenance operations, we will develop a secondary DT to accurately predict the near future axial tension. To these aims,

we will leverage operational data collected from the world's first commercial floating-wind farm (the Hywind Pilot Park) to investigate the effectiveness of DTs for the prediction of the MoL axial tension for the two scenarios depicted above. The DTs will be developed using state-of-the-art data-driven methods (Shalev-Shwartz and Ben-David 2014; Oneto 2020) and results based on real operational data will support our proposal.

The rest of the paper is organised as follows. Section 2 summarises the problem we aim to address and the related available dataset. Section 3 describes the proposed modelling approach, based on DDMs, to address the problem summarised in Section 2 using the previously described dataset. Section 4 reports the experimental results showing the effectiveness of our proposal. Finally, Section 5 concludes the paper.

2 Problem and dataset description

In this section, we will summarise the problems under investigation and the available data that can be exploited for building models able to address them.

In this work, we aim to face two problems: (i) detect long-term drifts in the mechanical response of the MoLs and (ii) predict the near future MoL axial tension.

For what concerns the first problem, as described in Sect. 1, we will develop a DT able to infer the expected behaviour of the MoLs in healthy conditions to compare with the actual one. Drifts in the differences between the actual and the predicted (healthy) behaviour are an indicator of decay in the condition of the MoL (Coraddu et al. 2019). This DT will take as inputs the current status of the factors influencing the MoL behaviour (i.e., the motions of the turbine and the environmental conditions) and as output the MoL axial tension.

When it comes to the second problem, as described in Sect. 1, we will develop another DT able to predict the near future axial tension utilising past and present factors (i.e., not only the motions of the turbine and the environmental conditions, but also the MoL tension), in combination with selected forecasted future factors (i.e., the environmental conditions) influencing the MoL behaviour.

Note the fundamental difference between the two DTs. In the first case, we just use instantaneous information (i.e., turbine's motions and the environmental conditions) to predict the axial tension as we want to compare the current response of the MoL with the (predicted) one that it would have in perfectly healthy conditions. Whereas, in the second case, we also use the "context" information (i.e., past, present, and forecasted data), since we want to develop an high fidelity system which is able to predict (both in healthy and decayed states) the responses of the MoL for safety concerns. In fact,

Table 2 Hywind data set (Catapult ORE 2020) features

Variable name	ID	Unit	Sampling rate (Hz)
Date–time	t	(s)	10
Drift (Easting)	D_e	(m)	10
Drift (Northing)	D_n	(m)	10
Nacelle pitch	θ_N	(rad)	10
Nacelle roll	ϕ_N	(rad)	10
Tower pitch	θ_T	(rad)	10
Tower roll	ϕ_T	(rad)	10
Tower Yaw	ψ_T	(rad)	1
Wind speed	v	(m/s)	10
Yaw girection	ψ_{dir}	(°)	10
Tension Line 1—Bridle 1	ML_1B_1	(kN)	5
Tension Line 1—Bridle 2	ML_1B_2	(kN)	5
Tension Line 2—Bridle 1	ML_2B_1	(kN)	5
Tension Line 2—Bridle 2	ML_2B_2	(kN)	5
Tension Line 3—Bridle 1	ML_3B_1	(kN)	5
Tension Line 3—Bridle 2	ML_3B_2	(kN)	5

also using past and forecasted data in the first scenario would compromise our ability to develop a system able not to "follow" the decaying behaviour of the MoLs (i.e., learn the expected healthy behaviour) (Coraddu et al. 2019).

To develop our DTs, we will exploit the publicly available Hywind dataset (Catapult ORE 2020). The dataset describes the weather, motion, and mooring line axial tension of an SWT-6.0-154 turbine floating in depths of between 95 and 120m, 25 km off the coast of Scotland. The dataset is composed of 11 intervals of the turbine motion and response, in 30 min windows over the course of 2018. Table 2 describes the features of the data set.

Table 3 reports the data collection periods together and the key operational information (i.e., the significant wave height H_s and the peak waves period T_p).

A schematic of the turbine and the relevant sensor placement is seen in Fig. 1.

3 Proposed approach

In the proposed context, predicting the axial tension of the FOWT MoLs, a general modelisation framework can be defined, characterised by an input space $\mathcal{X} \subseteq \mathbb{R}^d$, an output space $\mathcal{Y} \subseteq \mathbb{R}^b$, and an unknown relation $\mu : \mathcal{X} \rightarrow \mathcal{Y}$ to be learned (Shalev-Shwartz and Ben-David 2014; Hamilton 1994). For what concerns this work, \mathcal{X} is composed by the the motions of the turbine and the environmental conditions (i.e., D_e , D_n , θ_N , ϕ_N , θ_T , ϕ_T , ψ_T , v , and ψ_{dir} in Table 2), while the output space \mathcal{Y} refers to the axial tensions of the

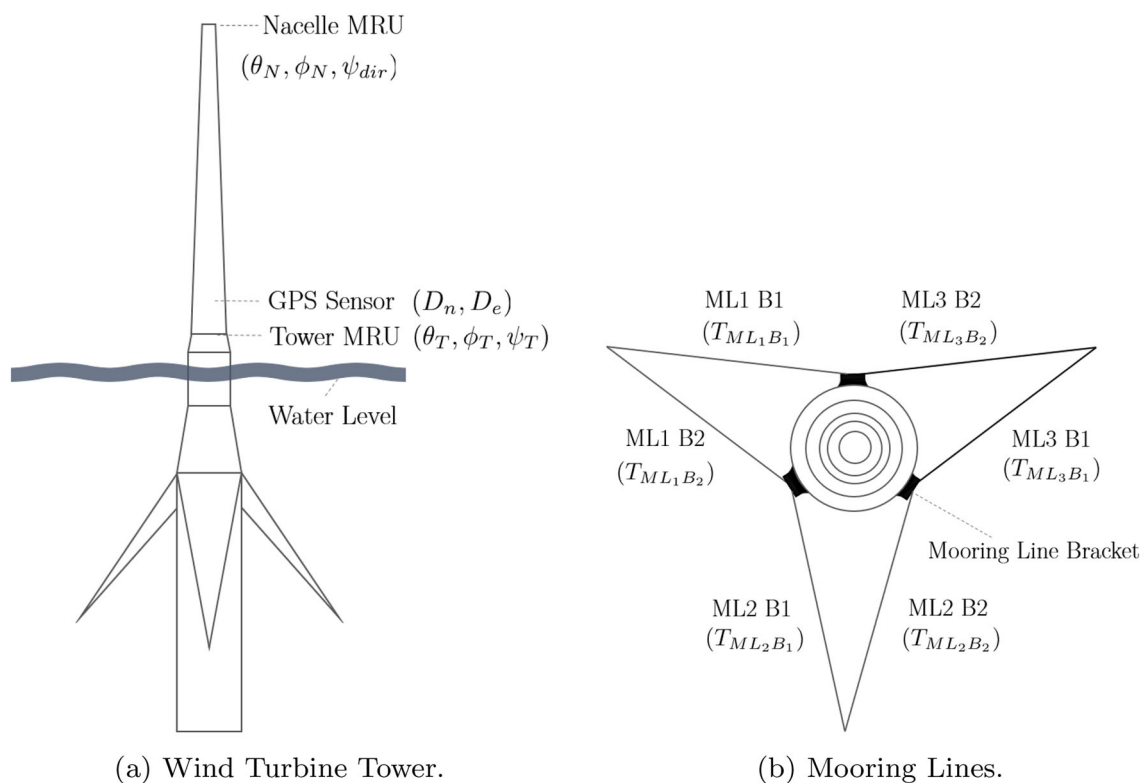


Fig. 1 Schematic of an FOWT including the relevant sensor placement for the features described in Table 2

Table 3 Hywind data set (Catapult ORE 2020) data collection periods together, and the key operational information

Interval	Date–time range	H_s (m)	T_p (s)
1	2018-03-26 23:15–23:45	2.23	10.6
2	2018-01-14 15:25–15:55	4.21	8.7
3	2018-04-14 00:25–00:55	2.07	10.5
4	2018-02-13 01:05–01:35	2.13	6.5
5	2018-02-24 04:35–05:05	2.51	7.3
6	2018-01-09 09:25–09:55	3.25	9.3
7	2018-01-06 07:45–08:15	4.41	10.9
8	2018-07-29 03:45–04:15	3.02	7.85
9	2018-05-02 03:15–04:45	2.28	6.5
10	2018-01-24 11:15–11:45	3.87	8.3
11	2018-01-24 11:25–11:55	3.85	8.3

FOWT MoL bridles (i.e., $T_{ML_1B_1}$, $T_{ML_1B_2}$, $T_{ML_2B_1}$, $T_{ML_2B_2}$, $T_{ML_3B_1}$, and $T_{ML_3B_2}$ in Table 2).

In this context, the authors define the model $h : \mathcal{X} \rightarrow \mathcal{Y}$ as an artificial simplification of μ . Now, the model h represents a DT of the FOWT MoL bridles. In our work, we aim to develop two kinds of DT (see Sect. 2):

- the first one to infer the expected behaviour of the MoLs in healthy conditions to compare with the actual one;

- the second one able to predict the near future axial tension utilising past and present factors.

The two DTs differ in the input space \mathcal{X} and the output space (see Fig. 2).

For what concerns the first DT, the input space is composed by instantaneous information at time t (i.e., D_e , D_n , θ_N , ϕ_N , θ_T , ϕ_T , ψ_T , v , and ψ_{dir} in Table 2), while the output space is the axial tensions of the FOWT MoL bridles at time t (i.e., $T_{ML_1B_1}$, $T_{ML_1B_2}$, $T_{ML_2B_1}$, $T_{ML_2B_2}$, $T_{ML_3B_1}$, and $T_{ML_3B_2}$ in Table 2). For what concerns the second DT, the input space is composed by past information during the time frame $[t - \Delta^-, t]$ (i.e., D_e , D_n , θ_N , ϕ_N , θ_T , ϕ_T , ψ_T , v , ψ_{dir} , $T_{ML_1B_1}$, $T_{ML_1B_2}$, $T_{ML_2B_1}$, $T_{ML_2B_2}$, $T_{ML_3B_1}$, and $T_{ML_3B_2}$ in Table 2) and the forecasted information $(t, t + \Delta^+]$ (i.e., D_e , D_n , and v , in Table 2) of the environmental conditions provided by a weather service, while the output space is the axial tensions of the FOWT MoL bridles at time $t + \Delta^+$. Δ^- represents how much history of the different available data we want to exploit to make predictions. Δ^+ , instead, represents the horizon of prediction. Δ^- is an hyperparameter for which an optimal value exists: too much history (too large Δ^-) will make us face with the curse of dimensionality, while too little history (too small Δ^-) will limit our ability to make accurate predictions (Shalev-Shwartz and Ben-David 2014; Oneto 2020; Hamilton 1994). Δ^+ , instead, depends on

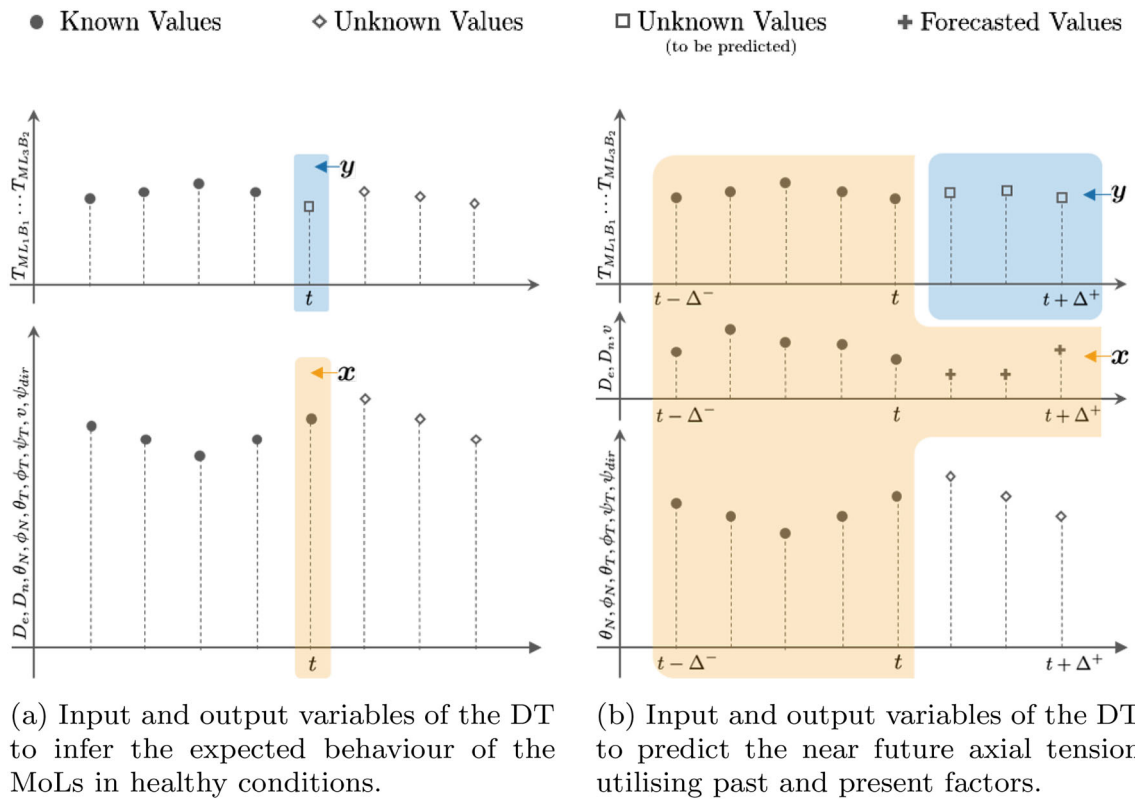


Fig. 2 Proposed DTs to account for the past and present available information to detect long-term drifts in the mechanical response of the MoLs and predict the near future MoL axial tension as described in Sect. 3

the application: usually, the larger the better but the more we try to forecast deep into the future, the less accurate the prediction will be (Shalev-Shwartz and Ben-David 2014; Oneto 2020; Hamilton 1994).

The model h , as described in Sect. 1 can be obtained with different kinds of techniques, for example, requiring some physical knowledge of the problem, as in PMs, or the acquisition of large amounts of data, as in DDMs. In this paper, we will use a state-of-the-art DDM for the reasons described in Sect. 1. Between the DDMs, it is possible to identify two families of approaches (Shalev-Shwartz and Ben-David 2014; Goodfellow et al. 2016). The first one, comprising traditional Machine Learning methods, needs an initial phase where the features must be defined a-priori from the data via feature engineering or implicit or explicit feature mapping (Shalev-Shwartz and Ben-David 2014; Zheng and Casari 2018; Shawe-Taylor and Cristianini 2004). The second family, which includes deep learning methods, automatically learns both the features and the models from the data Goodfellow et al. (2016). For small cardinality datasets and outside particular applications (e.g., computer vision and natural language processing), Deep Learning does not perform well, since they require huge amount of data to be reliable and to outperform traditional Machine Learn-

ing models (Fernández-Delgado et al. 2014; Wainberg et al. 2016).

Machine Learning maps the problem of building the two DTs in a typical regression problem (Vapnik 1998; Shawe-Taylor and Cristianini 2004). In fact, ML techniques aim at estimating the unknown relationship μ between input and output through a learning algorithm $\mathcal{A}_{\mathcal{H}}$ which exploits some historical data to learn h and where \mathcal{H} is a set of hyperparameters which characterises the generalisation performance of \mathcal{A} (Oneto 2020). The historical data consist on a series of n examples of the input/output relation μ and are defined as $\mathcal{D}_n = \{(\mathbf{x}_1, \mathbf{y}_1), \dots, (\mathbf{x}_n, \mathbf{y}_n)\}$ where $\mathbf{x} \in \mathcal{X}$ and $\mathbf{y} \in \mathcal{Y}$. For simplicity, we will indicate with y one of the elements in \mathbf{y} , since predicting a series of targets is equivalent to make a model for each one of the targets (Shalev-Shwartz and Ben-David 2014).

In this paper, we will leverage on a machine learning model coming from the Kernel methods family called Kernel regularised least squares (KRLS) (Vovk 2013). The idea behind KRLS can be summarised as follows. During the training phase, the quality of the learned function $h(\mathbf{x})$ is measured according to a loss function $\ell(h(\mathbf{x}), y)$ (Rosasco

et al. 2004) with the empirical error

$$\hat{L}_n(h) = \frac{1}{n} \sum_{i=1}^n \ell(h(\mathbf{x}_i), y_i). \tag{1}$$

A simple criterion for selecting the final model during the training phase could then consist in simply choosing the approximating function that minimises the empirical error $\hat{L}_n(h)$. This approach is known as empirical risk minimization (ERM) (Vapnik 1998). However, ERM is usually avoided in machine learning as it leads to severe overfitting of the model on the training dataset. As a matter of fact, in this case, the training process could choose a model, complicated enough to perfectly describe all the training samples (including the noise, which afflicts them). In other words, ERM implies memorisation of data rather than learning from them. A more effective approach is to minimise a cost function where the trade-off between accuracy on the training data and a measure of the complexity of the selected model is achieved (Tikhonov and Arsenin 1979), implementing the Occam’s razor principle

$$h^* : \min_h \hat{L}_n(h) + \lambda C(h). \tag{2}$$

In other words, the best approximating function h^* is chosen as the one that is complicated enough to learn from data without overfitting them. In particular, $C(\cdot)$ is a complexity measure: depending on the exploited machine learning approach, different measures are realised. Instead, $\lambda \in [0, \infty)$ is a hyperparameter, that must be set a-priori and is not obtained as an output of the optimisation procedure: it regulates the trade-off between the overfitting tendency, related to the minimisation of the empirical error, and the underfitting tendency, related to the minimisation of $C(\cdot)$. The optimal value for λ is problem-dependent, and tuning this hyperparameter is a non-trivial task, as will be discussed later in this section. In KRLS, models are defined as

$$h(\mathbf{x}) = \mathbf{w}^T \boldsymbol{\varphi}(\mathbf{x}), \tag{3}$$

where $\boldsymbol{\varphi}$ is an a-priori defined Feature Mapping (FM) (Shalev-Shwartz and Ben-David 2014) allowing to keep the structure of $h(\mathbf{x})$ linear. The complexity of the models, in KRLS, is measured as

$$C(h) = \|\mathbf{w}\|^2, \tag{4}$$

i.e., the Euclidean norm of the set of weights describing the regressor, which is a standard complexity measure in ML (Shalev-Shwartz and Ben-David 2014; Vovk 2013). Regarding the loss function, the square loss is typically

adopted because of its convexity, smoothness, and statistical properties (Rosasco et al. 2004)

$$\hat{L}_n(h) = \frac{1}{n} \sum_{i=1}^n \ell(h(\mathbf{x}_i), y_i) = \frac{1}{n} \sum_{i=1}^n [h(\mathbf{x}_i) - y_i]^2. \tag{5}$$

Consequently, Problem (2) can be reformulated as

$$\mathbf{w}^* : \min_{\mathbf{w}} \sum_{i=1}^n [\mathbf{w}^T \boldsymbol{\varphi}(\mathbf{x}_i) - y_i]^2 + \lambda \|\mathbf{w}\|^2. \tag{6}$$

By exploiting the Representer Theorem (Schölkopf et al. 2001), the solution h^* of the Problem (6) can be expressed as a linear combination of the samples projected in the space defined by $\boldsymbol{\varphi}$

$$h^*(\mathbf{x}) = \sum_{i=1}^n \alpha_i \boldsymbol{\varphi}(\mathbf{x}_i)^T \boldsymbol{\varphi}(\mathbf{x}). \tag{7}$$

It is worth underlining that, according to the kernel trick, it is possible to reformulate $h^*(\mathbf{x})$ without an explicit knowledge of $\boldsymbol{\varphi}$, and consequently avoiding the curse of dimensionality of computing $\boldsymbol{\varphi}$, using a proper kernel function $K(\mathbf{x}_i, \mathbf{x}) = \boldsymbol{\varphi}(\mathbf{x}_i)^T \boldsymbol{\varphi}(\mathbf{x})$

$$h^*(\mathbf{x}) = \sum_{i=1}^n \alpha_i K(\mathbf{x}_i, \mathbf{x}). \tag{8}$$

Several kernel functions can be retrieved in the literature (Scholkopf 2001; Cristianini and Shawe-Taylor 2000), each one with a particular property that can be exploited based on the problem under exam. Usually, the Gaussian kernel is chosen

$$K(\mathbf{x}_i, \mathbf{x}) = e^{-\gamma \|\mathbf{x}_i - \mathbf{x}\|^2}, \tag{9}$$

because of the theoretical reasons described in Keerthi and Lin (2003); Oneto et al. (2015) and because of its effectiveness (Fernández-Delgado et al. 2014; Wainberg et al. 2016). γ is another hyperparameter, which regulates the non-linearity of the solution that must be tuned as explained later. Basically, the Gaussian kernel is able to implicitly create an infinite-dimensional $\boldsymbol{\varphi}$, and thanks to this, the KRLS are able to learn any possible function (Keerthi and Lin 2003). The KRLS problem of Eq. (6) can be reformulated by exploiting kernels as

$$\boldsymbol{\alpha}^* : \min_{\boldsymbol{\alpha}} \|\mathbf{Q}\boldsymbol{\alpha} - \mathbf{y}\|^2 + \lambda \boldsymbol{\alpha}^T \mathbf{Q}\boldsymbol{\alpha}, \tag{10}$$

where $\mathbf{y} = [y_1, \dots, y_n]^T$, $\boldsymbol{\alpha} = [\alpha_1, \dots, \alpha_n]^T$, the matrix \mathbf{Q} such that $Q_{i,j} = K(\mathbf{x}_j, \mathbf{x}_i)$, and the identity matrix $\mathbf{I} \in$

$\mathbb{R}^{n \times n}$. By setting the gradient equal to 0 w.r.t. α , it is possible to state that

$$(Q + \lambda I) \alpha^* = y, \tag{11}$$

which is a linear system for which effective solvers have been developed over the years, allowing it to cope with even very large sets of training data (Young 2003).

Note that the computational complexity of making the prediction for a new point, see Eq. (8), increases with the number of samples in the training dataset. Nevertheless, in this paper, we did not focus on this specific issue which can be addressed in many ways, but we focus our attention on the ability of making accurate predictions. In fact, the simplest way to reduce the computational requirements of the prediction phase is to sub-sample the training set (as one can observe also from the results of Sect. 4, we do not need so much data to achieve high accuracy) with some advanced method as reported in (Aupetit 2009). Another method is to use a different loss, such as the epsilon-insensitive one (Shawe-Taylor and Cristianini 2004), to reduce the number of points actually used by the training model.

The problems we still have to face is how to tune the hyperparameters for this approach (λ , γ , and Δ^- for the second DT) and how to estimate the performance of the final model. Model selection (MS) and error estimation (EE) deal exactly with these problems (Oneto 2020). Resampling techniques are commonly used by researchers and practitioners, since they work well in most situations, and this is why, we will exploit them in this work (Oneto 2020). Other alternatives exist, based on the statistical learning theory, but they tend to underperform resampling techniques in practice (Oneto 2020). Resampling techniques are based on a simple idea: the original dataset \mathcal{D}_n is resampled once or many (n_r) times, with or without replacement, to build three independent datasets called learning, validation, and test sets, respectively \mathcal{L}_l^r , \mathcal{V}_v^r , and \mathcal{T}_t^r , with $r \in \{1, \dots, n_r\}$, such that

$$\mathcal{L}_l^r \cap \mathcal{V}_v^r = \emptyset, \quad \mathcal{L}_l^r \cap \mathcal{T}_t^r = \emptyset, \quad \mathcal{V}_v^r \cap \mathcal{T}_t^r = \emptyset \tag{12}$$

$$\mathcal{L}_l^r \cup \mathcal{V}_v^r \cup \mathcal{T}_t^r = \mathcal{D}_n. \tag{13}$$

Subsequently, to select the best hyperparameters' combination $\mathcal{H} = \{\lambda, \gamma, (\Delta^-)\}$ in a set of possible ones $\mathfrak{H} = \{\mathcal{H}_1, \mathcal{H}_2, \dots\}$ for the algorithm $\mathcal{A}_{\mathcal{H}}$ or, in other words, to perform the MS phase, the following procedure has to be applied:

$$\mathcal{H}^* : \arg \min_{\mathcal{H} \in \mathfrak{H}} \sum_{r=1}^{n_r} M(\mathcal{A}_{\mathcal{H}}(\mathcal{L}_l^r), \mathcal{V}_v^r), \tag{14}$$

where $h = \mathcal{A}_{\mathcal{H}}(\mathcal{L}_l^r)$ is a model built with the algorithm \mathcal{A} with its set of hyperparameters \mathcal{H} and with the data \mathcal{L}_l^r , and

where $M(h, \mathcal{V}_v^r)$ is a desired metric. Since the data in \mathcal{L}_l^r are independent from the data in \mathcal{V}_v^r , \mathcal{H}^* should be the set of hyperparameters which allows achieving a small error on a data set that is independent from the training set. Then, to evaluate the performance of the optimal model which is $h_{\mathcal{A}}^* = \mathcal{A}_{\mathcal{H}^*}(\mathcal{D}_n)$ or, in other words, to perform the EE phase, the following procedure has to be applied:

$$M(h_{\mathcal{A}}^*) = \frac{1}{n_r} \sum_{r=1}^{n_r} M(\mathcal{A}_{\mathcal{H}^*}(\mathcal{L}_l^r \cup \mathcal{V}_v^r), \mathcal{T}_t^r). \tag{15}$$

Since the data in $\mathcal{L}_l^r \cup \mathcal{V}_v^r$ are independent from the ones in \mathcal{T}_t^r , $M(h_{\mathcal{A}}^*)$ is an unbiased estimator of the true performance, measured with the metric M , of the final model Oneto (2020). In this work, we will rely on Complete k -fold cross-validation which means setting $n_r \leq \binom{n}{k} \binom{n-k}{k}$, $l = (k-2)\frac{n}{k}$, $v = \frac{n}{k}$, and $t = \frac{n}{k}$ and the resampling must be done without replacement (Oneto 2020). Note that, in our application, we have a further constraint in terms of dependence in time between the samples. For this reason, when resampling the data form \mathcal{D}_n , we actually keep data of different periods in \mathcal{L}_l^r , \mathcal{V}_v^r , and \mathcal{T}_t^r (Hamilton 1994).

For what concerns the metric M that we will use in our paper, we will rely on the mean absolute error (MAE) which computes the average absolute distance between the prediction and the actual value to predict (Willmott and Matsuura 2005). Since in regression, it is quite hard to synthesise the quality of a predictor in a single metric, we will also rely on visualisation techniques like the scatter plot (Shao et al. 2017) (see Sect. 4).

4 Experimental results

This section is devoted to the presentation of the results of applying and testing the methodology described in Sect. 3 leveraging on the data presented in Sect. 2.

As first step, we have to report the hyperparameters ranges of the MS phase which is common to all experiments. The set of hyperparameters tuned during the MS phase is $\mathcal{H} = \{\gamma, \lambda\}$ chosen in $\mathfrak{H} = \{10^{-4.0}, 10^{-3.8}, \dots, 10^{+4.0}\} \times \{10^{-4.0}, 10^{-3.8}, \dots, 10^{+4.0}\}$. For the second DT, we also investigated the effect of $\Delta^+ \in \{1, 2, 4, 8, 16, 32, 64, 128\}$ and $\Delta^- \in \{1, 2, 5, 10, 20\}$. For the second DT, Δ^- has also been tuned during the MS phase. All of the tests have been repeated 30 times, and the average results are reported together with their t-student 95% confidence interval, to ensure the statistical validity of the results.

Table 4 First DT: MAE for the different MoLs and bridles

ML ₁ B ₁	ML ₁ B ₂	ML ₂ B ₁	ML ₂ B ₂	ML ₃ B ₁	ML ₃ B ₂
11.4±0.1	11.6±0.1	14.7±0.1	22.9±0.2	12.2±0.2	12.5±0.1

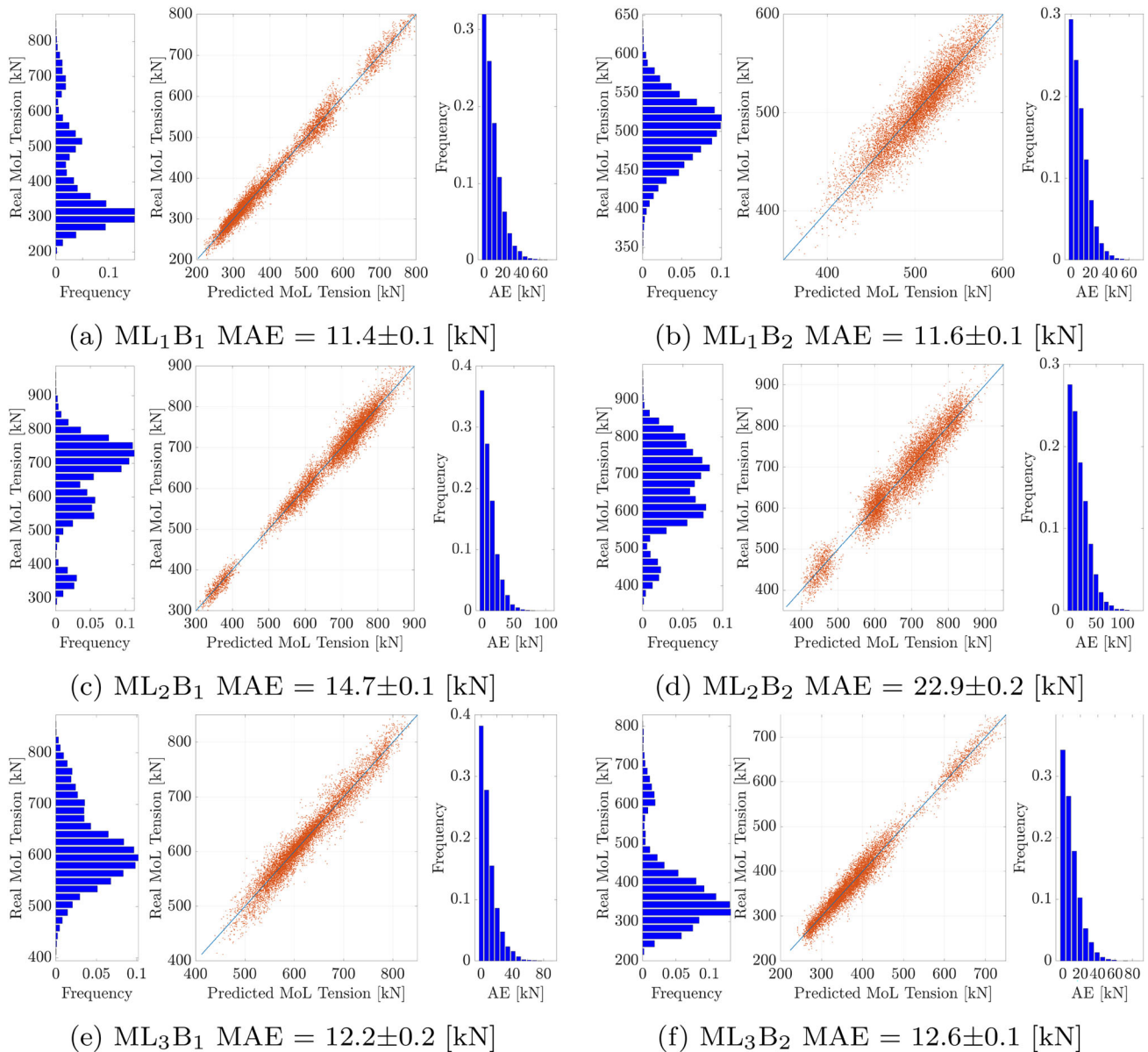


Fig. 3 First DT: scatter plot (real versus predicted) the real distribution, and the error distribution for the axial tension of the different MoLs and bridles

4.1 First digital twin

The first DT was designed to predict the MoL tension in healthy conditions to monitor the drift between the expected and true behaviour. This DT has to predict the instantaneous MoL tension from the current factors influencing the MoLs (i.e., the motions of the turbine and the environmental conditions) to accurately forecast the MoLs tension.

Table 4 reports the MAE of this first DT for the different MoLs and bridles.

Moreover, Fig. 3 reports the scatter plot (Real versus Predicted) the real distribution, and the error distribution for the axial tension of the different MoLs and bridles.

From Table 4 and Fig. 3, it is possible to observe that the proposed DT is able to accurately predict the MoL tension in healthy conditions from the current factors influencing

Fig. 4 Second DT: scatter plot (real versus predicted), real distribution, error distribution, and a piece of trend in time (real versus predicted) of the axial tension of the different MoLs and bridles with Δ^+ fixed at 64 (more the 1 min) as it is a sufficient time horizon for providing a reasonable warning to avoid accidents and Δ^- fixed to the optimal value according to Table 7

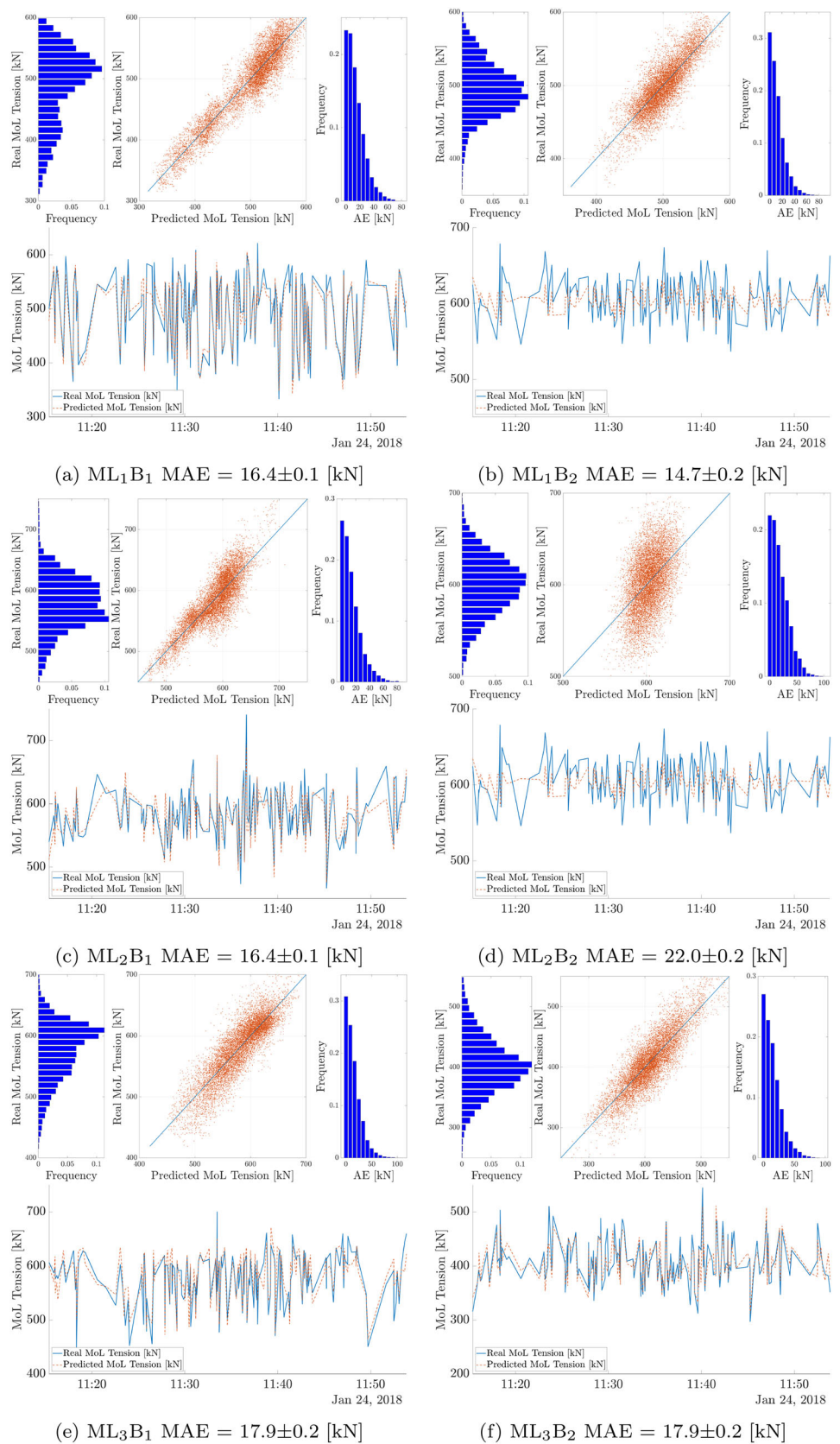


Fig. 5 Second DT: scatter plot (real versus predicted), real distribution, error distribution, and a piece of trend in time (real versus predicted) of the axial tension of the ML_1B_1 varying Δ^+ , with Δ^- fixed to the optimal value according to Table 7

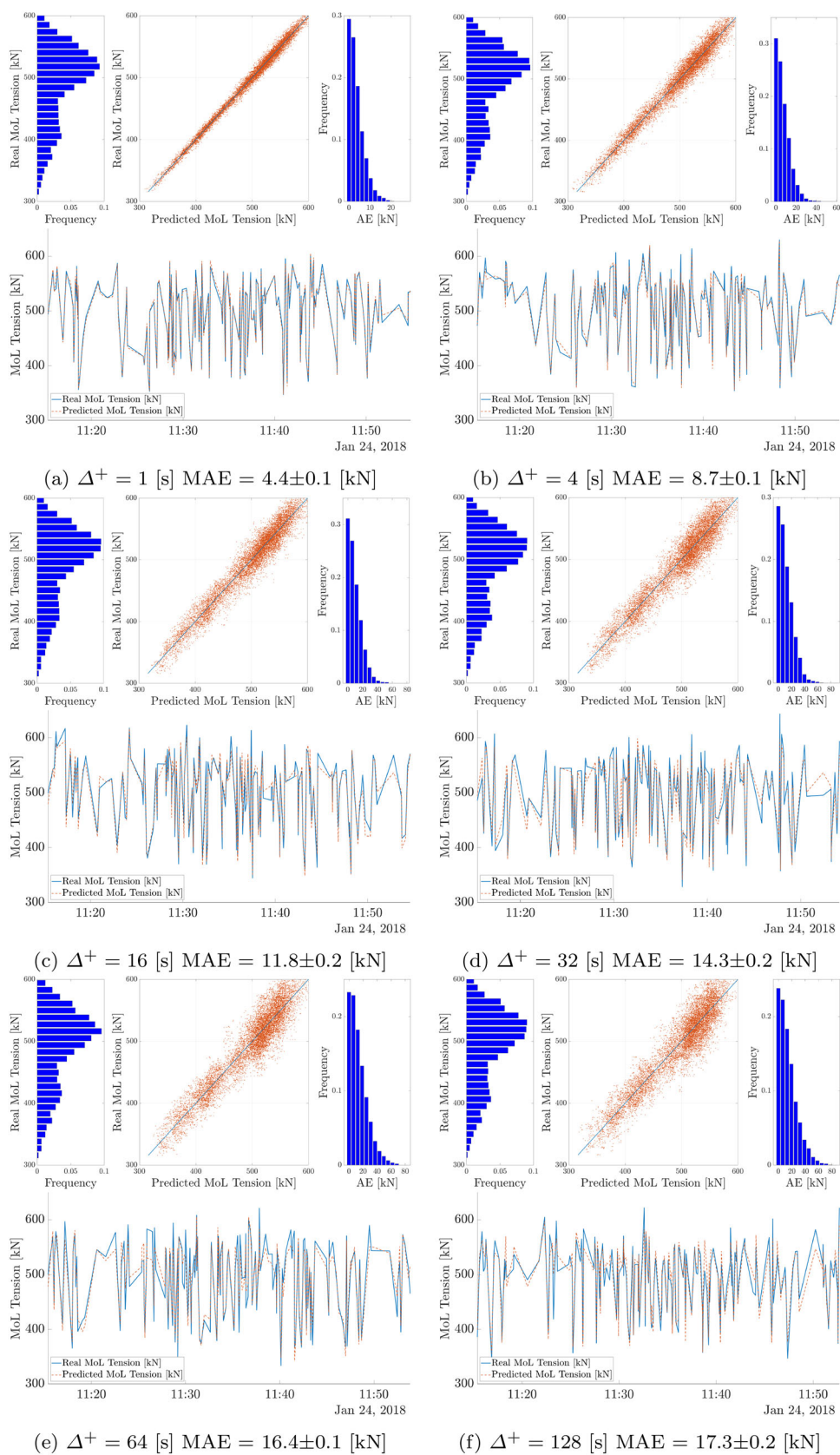


Table 5 Second DT: MAE of the proposed model varies changing Δ^- for different values of Δ^+

Δ^+ (s)	Δ^- (s)	ML ₁ B ₁	ML ₁ B ₂	ML ₂ B ₁	ML ₂ B ₂	ML ₃ B ₁	ML ₃ B ₂
1	1	5.3 ± 0.1	6.1 ± 0.1	7.8 ± 0.1	16.0 ± 0.2	6.5 ± 0.1	6.8 ± 0.1
	2	4.8 ± 0.1	5.9 ± 0.1	7.5 ± 0.1	16.2 ± 0.2	6.1 ± 0.1	6.6 ± 0.1
	5	4.5 ± 0.1	5.5 ± 0.1	6.9 ± 0.1	15.9 ± 0.2	6.0 ± 0.1	6.4 ± 0.1
	10	4.4 ± 0.1	5.4 ± 0.1	7.0 ± 0.1	15.4 ± 0.1	5.9 ± 0.1	6.2 ± 0.1
	20	4.6 ± 0.1	5.4 ± 0.0	7.0 ± 0.1	15.3 ± 0.2	5.9 ± 0.1	6.3 ± 0.1
2	1	9.0 ± 0.1	8.5 ± 0.1	10.5 ± 0.1	17.8 ± 0.2	8.9 ± 0.2	9.1 ± 0.1
	2	8.5 ± 0.1	7.9 ± 0.1	9.3 ± 0.1	17.3 ± 0.2	8.3 ± 0.1	8.7 ± 0.1
	5	7.6 ± 0.1	7.2 ± 0.1	8.7 ± 0.1	16.8 ± 0.2	7.8 ± 0.1	8.1 ± 0.1
	10	7.3 ± 0.1	7.0 ± 0.1	8.6 ± 0.1	16.4 ± 0.2	7.7 ± 0.1	7.9 ± 0.1
	20	7.4 ± 0.1	6.9 ± 0.1	8.6 ± 0.1	16.5 ± 0.2	7.7 ± 0.1	7.7 ± 0.1
4	1	12.7 ± 0.1	10.1 ± 0.1	12.2 ± 0.2	19.5 ± 0.3	10.8 ± 0.2	12.1 ± 0.2
	2	11.4 ± 0.2	9.6 ± 0.1	11.1 ± 0.1	18.6 ± 0.2	10.2 ± 0.1	10.7 ± 0.1
	5	10.3 ± 0.1	9.0 ± 0.1	10.5 ± 0.2	17.6 ± 0.2	9.9 ± 0.1	9.8 ± 0.1
	10	9.4 ± 0.1	8.5 ± 0.1	9.9 ± 0.1	17.5 ± 0.1	9.7 ± 0.1	9.4 ± 0.1
	20	8.7 ± 0.1	8.4 ± 0.1	10.2 ± 0.1	16.9 ± 0.2	9.5 ± 0.1	9.0 ± 0.1
8	1	14.8 ± 0.2	10.8 ± 0.1	13.5 ± 0.1	19.6 ± 0.1	13.3 ± 0.2	15.6 ± 0.2
	2	12.6 ± 0.3	10.5 ± 0.1	12.9 ± 0.1	19.0 ± 0.2	12.4 ± 0.2	13.2 ± 0.2
	5	10.8 ± 0.1	10.2 ± 0.1	12.3 ± 0.2	18.6 ± 0.3	11.4 ± 0.2	11.3 ± 0.2
	10	9.9 ± 0.2	9.9 ± 0.1	12.0 ± 0.1	18.2 ± 0.2	11.0 ± 0.1	10.3 ± 0.2
	20	9.5 ± 0.2	9.8 ± 0.1	12.0 ± 0.2	17.9 ± 0.2	11.0 ± 0.1	9.8 ± 0.1
16	1	18.4 ± 0.2	12.2 ± 0.2	16.3 ± 0.3	21.5 ± 0.2	16.5 ± 0.2	20.5 ± 0.3
	2	16.5 ± 0.2	12.0 ± 0.1	15.1 ± 0.2	20.9 ± 0.1	15.6 ± 0.2	18.0 ± 0.2
	5	14.1 ± 0.2	11.7 ± 0.2	14.1 ± 0.2	20.4 ± 0.3	14.0 ± 0.2	14.9 ± 0.2
	10	12.5 ± 0.2	11.1 ± 0.2	13.7 ± 0.2	20.0 ± 0.2	13.1 ± 0.2	13.1 ± 0.2
	20	11.8 ± 0.2	10.9 ± 0.2	13.5 ± 0.2	20.1 ± 0.1	13.2 ± 0.2	12.6 ± 0.2
32	1	21.9 ± 0.3	14.3 ± 0.2	18.7 ± 0.2	23.2 ± 0.2	20.4 ± 0.3	26.7 ± 0.4
	2	19.8 ± 0.3	14.3 ± 0.2	17.6 ± 0.2	22.9 ± 0.3	19.2 ± 0.3	23.9 ± 0.3
	5	17.2 ± 0.3	14.2 ± 0.2	16.8 ± 0.2	22.9 ± 0.2	17.5 ± 0.2	20.0 ± 0.2
	10	15.3 ± 0.2	13.6 ± 0.2	15.9 ± 0.2	22.3 ± 0.4	16.7 ± 0.2	17.7 ± 0.3
	20	14.3 ± 0.2	13.3 ± 0.1	15.2 ± 0.2	21.9 ± 0.2	16.7 ± 0.2	16.4 ± 0.2
64	1	18.2 ± 0.2	15.3 ± 0.1	17.4 ± 0.3	23.1 ± 0.3	18.2 ± 0.3	19.6 ± 0.3
	2	17.4 ± 0.1	14.9 ± 0.2	17.4 ± 0.2	22.8 ± 0.3	18.2 ± 0.2	18.9 ± 0.3
	5	16.9 ± 0.3	14.7 ± 0.2	17.0 ± 0.2	22.6 ± 0.4	17.9 ± 0.2	18.5 ± 0.2
	10	16.6 ± 0.2	14.7 ± 0.3	16.9 ± 0.3	22.4 ± 0.2	17.9 ± 0.1	18.1 ± 0.2
	20	16.4 ± 0.1	14.8 ± 0.2	16.4 ± 0.1	22.0 ± 0.2	17.9 ± 0.2	17.9 ± 0.2
128	1	20.9 ± 0.2	16.1 ± 0.2	18.9 ± 0.3	23.7 ± 0.3	21.0 ± 0.3	24.7 ± 0.4
	2	19.8 ± 0.2	16.0 ± 0.2	18.5 ± 0.3	23.2 ± 0.4	20.9 ± 0.3	23.0 ± 0.3
	5	19.0 ± 0.2	15.9 ± 0.2	18.3 ± 0.3	22.8 ± 0.3	20.4 ± 0.3	21.5 ± 0.3
	10	17.9 ± 0.2	16.0 ± 0.2	18.2 ± 0.3	22.5 ± 0.3	20.4 ± 0.3	20.3 ± 0.3
	20	17.3 ± 0.2	15.7 ± 0.2	17.7 ± 0.3	22.4 ± 0.2	19.8 ± 0.4	19.9 ± 0.4

the MoLs (i.e., the motions of the turbine and the environmental conditions). In particular, with the exception of the ML₂B₂, the MAE error for the remaining 5 bridles is under 15 [kN] across our tests as reported in Table 4). At this point, it is important to remember that the dataset is composed of sporadic periods throughout the year (as described in Table 3) and such captures a wide range of operating con-

ditions (which is clear from the metocean features reported in the same table). Despite this wide range of operating conditions, the DTs exhibit small error variance, indicating that the models performed consistently well across all conditions. Figure 3 allows us to better understand the quality of the developed DTs, further supporting the discussion raised from the tabular results, showing the behaviour of the predictions

Table 6 Second DT: MAE of the proposed model as a function of Δ^+ for different values of Δ^-

Δ^+ (s)	Δ^- (s)	ML ₁ B ₁	ML ₁ B ₂	ML ₂ B ₁	ML ₂ B ₂	ML ₃ B ₁	ML ₃ B ₂
1	1	5.3 ± 0.1	6.1 ± 0.1	7.8 ± 0.1	16.0 ± 0.2	6.5 ± 0.1	6.8 ± 0.1
2		9.0 ± 0.1	8.5 ± 0.1	10.5 ± 0.1	17.8 ± 0.2	8.9 ± 0.2	9.1 ± 0.1
4		12.7 ± 0.1	10.1 ± 0.1	12.2 ± 0.2	19.5 ± 0.3	10.8 ± 0.2	12.1 ± 0.2
8		14.8 ± 0.2	10.8 ± 0.1	13.5 ± 0.1	19.6 ± 0.1	13.3 ± 0.2	15.6 ± 0.2
16		18.4 ± 0.2	12.2 ± 0.2	16.3 ± 0.3	21.5 ± 0.2	16.5 ± 0.2	20.5 ± 0.3
32		21.9 ± 0.3	14.3 ± 0.2	18.7 ± 0.2	23.2 ± 0.2	20.4 ± 0.3	26.7 ± 0.4
64		18.2 ± 0.2	15.3 ± 0.1	17.4 ± 0.3	23.1 ± 0.3	18.2 ± 0.3	19.6 ± 0.3
128		20.9 ± 0.2	16.1 ± 0.2	18.9 ± 0.3	23.7 ± 0.3	21.0 ± 0.3	24.7 ± 0.4
1	2	4.8 ± 0.1	5.9 ± 0.1	7.5 ± 0.1	16.2 ± 0.2	6.1 ± 0.1	6.6 ± 0.1
2		8.5 ± 0.1	7.9 ± 0.1	9.3 ± 0.1	17.3 ± 0.2	8.3 ± 0.1	8.7 ± 0.1
4		11.4 ± 0.2	9.6 ± 0.1	11.1 ± 0.1	18.6 ± 0.2	10.2 ± 0.1	10.7 ± 0.1
8		12.6 ± 0.3	10.5 ± 0.1	12.9 ± 0.1	19.0 ± 0.2	12.4 ± 0.2	13.2 ± 0.2
16		16.5 ± 0.2	12.0 ± 0.1	15.1 ± 0.2	20.9 ± 0.1	15.6 ± 0.2	18.0 ± 0.2
32		19.8 ± 0.3	14.3 ± 0.2	17.6 ± 0.2	22.9 ± 0.3	19.2 ± 0.3	23.9 ± 0.3
64		17.4 ± 0.1	14.9 ± 0.2	17.4 ± 0.2	22.8 ± 0.3	18.2 ± 0.2	18.9 ± 0.3
128		19.8 ± 0.2	16.0 ± 0.2	18.5 ± 0.3	23.2 ± 0.4	20.9 ± 0.3	23.0 ± 0.3
1	5	4.5 ± 0.1	5.5 ± 0.1	6.9 ± 0.1	15.9 ± 0.2	6.0 ± 0.1	6.4 ± 0.1
2		7.6 ± 0.1	7.2 ± 0.1	8.7 ± 0.1	16.8 ± 0.2	7.8 ± 0.1	8.1 ± 0.1
4		10.3 ± 0.1	9.0 ± 0.1	10.5 ± 0.2	17.6 ± 0.2	9.9 ± 0.1	9.8 ± 0.1
8		10.8 ± 0.1	10.2 ± 0.1	12.3 ± 0.2	18.6 ± 0.3	11.4 ± 0.2	11.3 ± 0.2
16		14.1 ± 0.2	11.7 ± 0.2	14.1 ± 0.2	20.4 ± 0.3	14.0 ± 0.2	14.9 ± 0.2
32		17.2 ± 0.3	14.2 ± 0.2	16.8 ± 0.2	22.9 ± 0.2	17.5 ± 0.2	20.0 ± 0.2
64		16.9 ± 0.3	14.7 ± 0.2	17.0 ± 0.2	22.6 ± 0.4	17.9 ± 0.2	18.5 ± 0.2
128		19.0 ± 0.2	15.9 ± 0.2	18.3 ± 0.3	22.8 ± 0.3	20.4 ± 0.3	21.5 ± 0.3
1	10	4.4 ± 0.1	5.4 ± 0.1	7.0 ± 0.1	15.4 ± 0.1	5.9 ± 0.1	6.2 ± 0.1
2		7.3 ± 0.1	7.0 ± 0.1	8.6 ± 0.1	16.4 ± 0.2	7.7 ± 0.1	7.9 ± 0.1
4		9.4 ± 0.1	8.5 ± 0.1	9.9 ± 0.1	17.5 ± 0.1	9.7 ± 0.1	9.4 ± 0.1
8		9.9 ± 0.2	9.9 ± 0.1	12.0 ± 0.1	18.2 ± 0.2	11.0 ± 0.1	10.3 ± 0.2
16		12.5 ± 0.2	11.1 ± 0.2	13.7 ± 0.2	20.0 ± 0.2	13.1 ± 0.2	13.1 ± 0.2
32		15.3 ± 0.2	13.6 ± 0.2	15.9 ± 0.2	22.3 ± 0.4	16.7 ± 0.2	17.7 ± 0.3
64		16.6 ± 0.2	14.7 ± 0.3	16.9 ± 0.3	22.4 ± 0.2	17.9 ± 0.1	18.1 ± 0.2
128		17.9 ± 0.2	16.0 ± 0.2	18.2 ± 0.3	22.5 ± 0.3	20.4 ± 0.3	20.3 ± 0.3
1	20	4.6 ± 0.1	5.4 ± 0.0	7.0 ± 0.1	15.3 ± 0.2	5.9 ± 0.1	6.3 ± 0.1
2		7.4 ± 0.1	6.9 ± 0.1	8.6 ± 0.1	16.5 ± 0.2	7.7 ± 0.1	7.7 ± 0.1
4		8.7 ± 0.1	8.4 ± 0.1	10.2 ± 0.1	16.9 ± 0.2	9.5 ± 0.1	9.0 ± 0.1
8		9.5 ± 0.2	9.8 ± 0.1	12.0 ± 0.2	17.9 ± 0.2	11.0 ± 0.1	9.8 ± 0.1
16		11.8 ± 0.2	10.9 ± 0.2	13.5 ± 0.2	20.1 ± 0.1	13.2 ± 0.2	12.6 ± 0.2
32		14.3 ± 0.2	13.3 ± 0.1	15.2 ± 0.2	21.9 ± 0.2	16.7 ± 0.2	16.4 ± 0.2
64		16.4 ± 0.1	14.8 ± 0.2	16.4 ± 0.1	22.0 ± 0.2	17.9 ± 0.2	17.9 ± 0.2
128		17.3 ± 0.2	15.7 ± 0.2	17.7 ± 0.3	22.4 ± 0.2	19.8 ± 0.4	19.9 ± 0.4

against the measured MoL tension by means of scatter plots and distributions of the measured MoL tension and errors. As one can observe from Fig. 3, the DTs consistently performs well across the different MoLs and bridles. Based on these results, we can safely state that the family of DTs we developed in this section would be well suited for monitoring

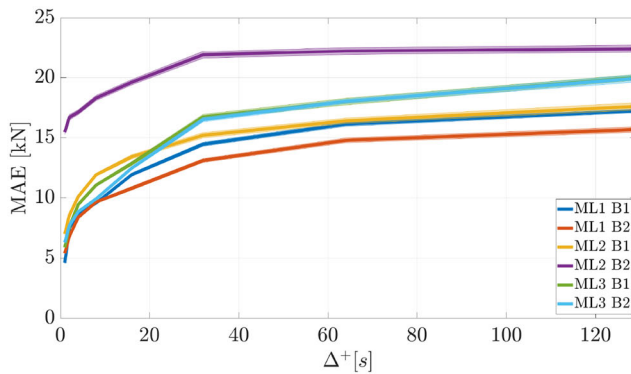
the health status of the MoLs by detecting drifts between the expected MoL tension and the real one.

4.2 Second digital twin

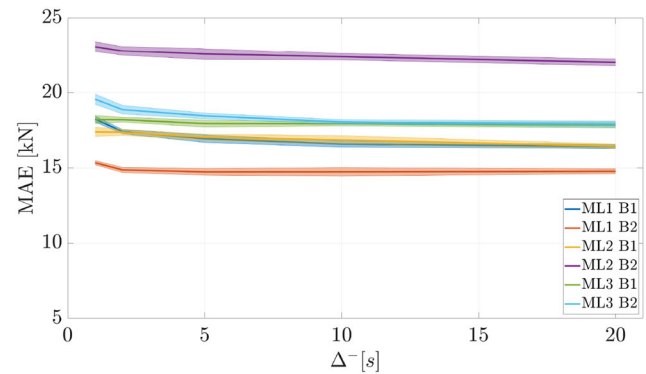
The second DT was designed to predict the near future axial tension, using past, present, and forecasted data to predict the

Table 7 Second DT: MAE when Δ^- is optimised during the MS phase for different values of Δ^+

Δ^+ (s)	ML ₁ B ₁	ML ₁ B ₂	ML ₂ B ₁	ML ₂ B ₂	ML ₃ B ₁	ML ₃ B ₂
1	4.4 ± 0.1	5.4 ± 0.1	6.9 ± 0.1	15.3 ± 0.2	5.9 ± 0.1	6.2 ± 0.1
2	7.3 ± 0.1	6.9 ± 0.1	8.6 ± 0.1	16.4 ± 0.2	7.7 ± 0.1	7.7 ± 0.1
4	8.7 ± 0.1	8.4 ± 0.1	9.9 ± 0.1	16.9 ± 0.2	9.5 ± 0.1	9.0 ± 0.1
8	9.5 ± 0.2	9.8 ± 0.1	12.0 ± 0.2	17.9 ± 0.2	11.0 ± 0.1	9.8 ± 0.1
16	11.8 ± 0.2	10.9 ± 0.2	13.5 ± 0.2	20.0 ± 0.2	13.1 ± 0.2	12.6 ± 0.2
32	14.3 ± 0.2	13.3 ± 0.1	15.2 ± 0.2	21.9 ± 0.2	16.7 ± 0.2	16.4 ± 0.2
64	16.4 ± 0.1	14.7 ± 0.2	16.4 ± 0.1	22.0 ± 0.2	17.9 ± 0.2	17.9 ± 0.2
128	17.3 ± 0.2	15.7 ± 0.2	17.7 ± 0.3	22.4 ± 0.2	19.8 ± 0.4	19.9 ± 0.4



(a) $\Delta^- = 20$ [s] and varying Δ^+ .



(b) $\Delta^+ = 64$ [s] and varying Δ^- .

Fig. 6 Second DT: MAE of the different MoLs and bridles when fixing $\Delta^- = 20$ (the value of Δ^- which most commonly is the optimal one according to Table 7) and varying Δ^+ , when Δ^+ is fixed at 64 (the most reasonable time horizon to be able to avoid accidents) and varying Δ^-

near future MoL tension for safety purposes (e.g., control and maintenance activities).

Table 5 shows how the MAE of the proposed model varies changing Δ^- for different values of Δ^+ . Vice versa, Table 6 shows the MAE's variation of the proposed model as a function of Δ^+ for different values of Δ^- . It is worth mentioning that Tables 5 and 6 actually contain the same information but presented in different ways for the sake of readability. Finally, Tables 7 reports the MAE when Δ^- is optimised during the MS phase for different values of Δ^+ .

Analogously to the results shown in Sect. 4.1, we have reported a series of pictures to improve and enrich the ability of the reader to understand the real performance of the developed models, as in regression, it is harder to synthesise the quality of the model just with a single metric (as we did in Tables 5, 6, and 7). For this reason, Fig. 4 reports the scatter plot (Real versus Predicted), real distribution, error distribution, and a snapshot of the trend in time (real and predicted) of the axial tension for the different MoLs and bridles with Δ^+ fixed at 64 s (more the 1 min). In fact, this represents a sufficient time horizon for providing a reasonable warning and fixing Δ^- to the optimal value according to Table 7. Then, Fig. 5 reports scatter plot (real versus predicted), real distribution, error distribution, and a snapshot

of the trend in time (real and predicted) of the axial tension of the ML₁B₁ varying Δ^+ fixing Δ^- to the optimal value according to Table 7. Finally, Fig. 6 reports how the MAE varies in predicting the axial tension of the different MoLs and bridles when fixing $\Delta^- = 20$ (the value of Δ^- which most commonly is the optimal one according to Table 7) and varying Δ^+ and when fixing $\Delta^+ = 64$ (the most reasonable time horizon to be able to avoid accidents) and varying Δ^- .

From Table 5, 6, and 7 and from Figs. 4 and 5, it is possible to observe that

- as expected from the theory, observing from Tables 5 and 6, an optimal value for Δ^- exists to provide enough information to learn the current behaviour of the MoLs and forecast the tension accurately;
- as for the prediction horizon (Δ^+), the more we increase it, the higher is the prediction error (see Tables 5 and 6) which is again inline with one would expect. The performance's decrease caused by the increase in the prediction horizon is reported in Fig. 6. For small Δ^+ , as one may expect, the errors are very low (MAE $\approx 5/10$ kN). The model performance for the horizon we are interested for practical applications ($\approx 1/2$ min) is good enough (MAE $\approx 15/20$ kN) as reported in Table 7;

- there is a very good agreement between the real and predicted MoL tension as reported in Fig. 4. This demonstrates that the models were effective at learning the short-term behaviour of the MoLs.

In conclusion, results indicate that this second family of DTs proved to be an effective tool for operators to utilise where a time-sensitive response to the state of the MoLs is required.

5 Conclusions

The number of installed FOWTs has exponentially grown in the last decade, quadrupling the total installed capacity. This growth is expected to continue in the next decade leading to an increasing need to address main challenges for FOWT projects: monitoring the system's integrity, extending the lifespan of the components, and maintaining FOWTs safely at scale. Effectively and efficiently addressing these challenges would unlock the wider-scale deployment of FOWTs.

For these reasons, in this work, we developed two DTs to predict the MoL tension of an FOWT exploiting state-of-the-art data-driven methods and leveraging the data coming from the Hywind Pilot Park to test our proposals. The first DT was able to predict the MoL tension under healthy conditions to monitor the drift between the expected and true behaviour. This DT represents an effective solution to detect long-term drifts in the mechanical response of the MoLs, and accurately predict the behaviour of the healthy system to compare with the actual one. The second DT utilised past, present, and forecasted data to predict the near future MoL tension for safety purposes. In particular, we were able to achieve good results (with an error of around 15 [kN]) for a forecast horizon of approximately 1–2 min, which is enough to better operated the FOWTs generate early safety-related warnings. By changing the FOWT operational settings, according to this second DT prediction, operators can increase the lifespan of the MoLs by reducing the actual mechanical stress and, additionally, in the case where FOWT operational maintenance is in progress, the prediction from the DT can serve as early safety warning to operators.

As a concluding remark, it is important to stress that this work is just a preliminary step forward validated on a limited amount of data. The commercial use of FOWTs is still in its infancy, and the available dataset only captures sporadic periods throughout the year. For this reason, more tests with a more extensive set of data need to be conducted. Moreover, these DTs need to be integrated into real monitoring,

control, and safety systems to validate the potentiality of the models.

Open Access This article is licensed under a Creative Commons Attribution 4.0 International License, which permits use, sharing, adaptation, distribution and reproduction in any medium or format, as long as you give appropriate credit to the original author(s) and the source, provide a link to the Creative Commons licence, and indicate if changes were made. The images or other third party material in this article are included in the article's Creative Commons licence, unless indicated otherwise in a credit line to the material. If material is not included in the article's Creative Commons licence and your intended use is not permitted by statutory regulation or exceeds the permitted use, you will need to obtain permission directly from the copyright holder. To view a copy of this licence, visit <http://creativecommons.org/licenses/by/4.0/>.

References

- ABSG Consulting (2015) Study on Mooring system integrity management for floating structures. <https://www.bsee.gov/sites/bsee.gov/files/tap-technical-assessment-program//730-aa.pdf>
- Al-Solihat MK, Nahon M (2018) Flexible multibody dynamic modeling of a floating wind turbine. *Int J Mech Sci* 142–143:518–529
- Angela A, Edwards G, Souza S, Gan TH (2017) Mooring integrity management: Novel approaches towards in situ monitoring. In: Rivas-Lopez M, Fuentes WF, Sergiyenko O (eds) *Structural Health Monitoring*, IntechOpen, Rijeka, chap 5
- Aranha JA, Pinto MO (2001) Dynamic tension in risers and mooring lines: An algebraic approximation for harmonic excitation. *Appl Ocean Res* 23(2):63–81
- Aupetit M (2009) Nearly homogeneous multi-partitioning with a deterministic generator. *Neurocomputing* 72(7–9):1379–1389
- Bhinder M, Karimirad M, Weller S, Debruyne Y, Guerinel M, Sheng W (2015) Modelling mooring line nonlinearities (material and geometric effects) for a wave energy converter using aqwa, sima and orcaflex. In: *Proceedings of the 11th European Wave and Tidal Energy Conference: EWTEC2015*
- Borg M, Collu M, Kolios A (2014) Offshore floating vertical axis wind turbines, dynamics modelling state of the art. Part II: Mooring line and structural dynamics. *Renew Sustain Energy Rev* 39:1226–1234
- Brown M, Hall T, Marr D, English M, Snell R (2005) Floating Production Mooring Integrity JIP - Key Findings. In: *OTC Offshore Technology Conference*
- Butterfield S, Musial W, Jonkman J, Sclavounos P (2005) Engineering challenges for floating offshore wind turbines. In: *Copenhagen Offshore Wind Conference*
- Carbon Trust (2015) Market and technology review. In: *Floating offshore wind*
- Carbon Trust (2018) Phase 1 summary report. In: *Floating Wind Joint Industry Project*
- Carbon Trust (2020) Phase 2 summary report. In: *Floating Wind Joint Industry Project*
- Catapult ORE (2020) Floating turbine design cases. <https://pod.ore.catapult.org.uk/data-collection/floating-turbine-design-cases>
- Cevasco D, Collu M, Rizzo CM, Hall M (2018) On mooring line tension and fatigue prediction for offshore vertical axis wind turbines: a comparison of lumped mass and quasi-static approaches. *Wind Eng* 42(2):97–107
- Coraddu A, Oneto L, Baldi F, Cipollini F, Atlar M, Savio S (2019) Data-driven ship digital twin for estimating the speed loss caused by the marine fouling. *Ocean Eng* 186(106):063

- Coraddu A, Oneto L, Cipollini F, Kalikatzarakis M (2020) Physical, data-driven, and hybrid approaches to model engine exhaust gas temperatures in operational conditions. *Ships Offshore Struct*
- Coraddu A, Oneto L, Ilardi D, Stoumpos S, Theotokatos G (2021) Marine dual fuel engines monitoring in the wild through weakly supervised data analytics. *Eng Appl Artif Intell* 100(104):179
- Cristianini N, Shawe-Taylor J (2000) An introduction to support vector machines and other kernel-based learning methods. Cambridge University Press, Cambridge
- Davidson J, Ringwood JV (2017) Mathematical modelling of mooring systems for wave energy converters—a review. *Energies* 10(5):666
- Fernández-Delgado M, Cernadas E, Barro S, Amorim D (2014) Do we need hundreds of classifiers to solve real world classification problems? *J Mach Learn Res* 15(1):3133–3181
- Fugro NV (2020) Fugro GB Marine Ltd. <https://www.fugro.com/>
- Goodfellow I, Bengio Y, Courville A (2016) Deep learning. MIT Press, Cambridge
- Hall M, Buckham B, Crawford C (2014) Evaluating the importance of mooring line model fidelity in floating offshore wind turbine simulations. *Wind Energy* 17(12):1835–1853
- Hamilton JD (1994) Time series analysis. Princeton University Press, Princeton
- Hannon M, Topham E, Dixon J, McMillan D, Collu M (2019) Offshore wind, ready to float? Global and UK trends in the floating offshore wind market. University of Strathclyde, Glasgow
- Hsu W, Thiagarajan K, Hall M, MacNicoll M, Akers R (2014) Snap Loads on Mooring Lines of a Floating Offshore Wind Turbine Structure. In: International Conference on Offshore Mechanics and Arctic Engineering, vol 9A: Ocean Renewable Energy
- Hsu W, Thiagarajan K, MacNicoll M, Akers R (2015) Prediction of Extreme Tensions in Mooring Lines of a Floating Offshore Wind Turbine in a 100-Year Storm. In: International Conference on Offshore Mechanics and Arctic Engineering, vol 9: Ocean Renewable Energy
- Hsu WT, Thiagarajan KP, Manuel L (2017) Extreme mooring tensions due to snap loads on a floating offshore wind turbine system. *Mar Struct* 55:182–199
- Jaiswal V, Ruskin A (2019) Mooring Line Failure Detection Using Machine Learning. In: OTC Offshore Technology Conference
- Jin C, Kim M (2018) Time-domain hydro-elastic analysis of a SFT (submerged floating tunnel) with Mooring lines under extreme wave and seismic excitations. *Appl Sci* 8:2386
- Karimirad M (2013) Modeling aspects of a floating wind turbine for coupled wave-wind-induced dynamic analyses. *Renew Energy* 53:299–305
- Keerthi SS, Lin CJ (2003) Asymptotic behaviors of support vector machines with gaussian kernel. *Neural Comput* 15(7):1667–1689
- Li CB, Choung J, Noh MH (2018) Wide-banded fatigue damage evaluation of Catenary mooring lines using various Artificial Neural Networks models. *Mar Struct* 60:186–200
- Wang S, Lu P (2016) On the Monitoring of Mooring System Performance. In: SNAME Offshore Symposium
- Ma G, Liang Z, Zhang X, Ma Q, Kang H (2020) Mechanism of mooring linebreakage of floating offshore wind turbine under extreme coherent gust with direction change condition. *J Mar Sci Technol* 25
- Ma K, Shu H, Smedley P, L'Hostis D, Duggal A (2013) A Historical Review on Integrity Issues of Permanent Mooring Systems. In: OTC Offshore Technology Conference
- Marin LifeLine (2021) Dry Mooring line monitoring for floating production systems. <https://www.marin.nl/jips/lifeline>
- Maroju S, Delaney K, Leon C, Prislis I (2013) Estimation of critical platform integrity parameters in the absence of direct measurements in the context of integrated marine monitoring systems. In: ASME 2013 32nd International Conference on Ocean, Offshore and Arctic Engineering
- Oneto L (2020) Model selection and error estimation in a Nutshell. Springer, New York
- Oneto L, Ghio A, Ridella S, Anguita D (2015) Support vector machines and strictly positive definite kernel: The regularization hyperparameter is more important than the kernel hyperparameters. In: IEEE international joint conference on neural networks (IJCNN)
- Oneto L, Coraddu A, Cipollini F, Karpenko O, Xepapa K, Sanetti P, Anguita D (2018) Crash stop maneuvering performance prediction: a data-driven solution for safety and collision avoidance. *Data Enabled Discov Appl* 2(1):1–11
- de Pina AC, de Pina AA, Albrecht CH, Pires L, de Lima BS, Jacob BP (2013) ANN-based surrogate models for the analysis of mooring lines and risers. *Appl Ocean Res* 41:76–86
- Prislis I, Maroju S (2017) Mooring Integrity and Machine Learning. In: OTC Offshore Technology Conference
- Qiao D, Yan J, Liang H, Ning D, Li B, Ou J (2020) Analysis on snap load characteristics of mooring line in slack-taut process. *Ocean Eng* 196(106):807
- Ren Z, Verma A, Li Y, Teuwen J, Jiang Z (2021) Offshore wind turbine operations and maintenance: A state-of-the-art review. *Renew Sustain Energy Rev* 144
- Rockmann C, Lagerveld S, Stavenuiter J (2017) Operation and maintenance costs of offshore wind farms and potential multi-use platforms in the dutch north sea. In: Buck B, Langan R (eds) Aquaculture perspective of multi-use sites in the open ocean, Springer, pp 97–113
- Rosasco L, De Vito E, Caponnetto A, Piana M, Verri A (2004) Are loss functions all the same? *Neural Comput* 16(5):1063–1076
- Santos F, Teixeira A, Guedes Soares C (2016) Operation and maintenance of floating offshore wind turbines. In: Floating Offshore Wind Farms, pp 181–193
- Schölkopf B (2001) The kernel trick for distances. In: Leen T, Dietterich T, Tresp V (eds) Advances in Neural Information Processing Systems, MIT Press, vol 13
- Schölkopf B, Herbrich R, Smola AJ (2001) A generalized representer theorem. In: Helmbold D, Williamson B (eds) Computational Learning Theory, Springer, Berlin, Heidelberg, pp 416–426
- Shalev-Shwartz S, Ben-David S (2014) Understanding machine learning: From theory to algorithms. Cambridge University Press, Cambridge
- Shao L, Mahajan A, Schreck T, Lehmann DJ (2017) Interactive regression lens for exploring scatter plots. In: Computer graphics forum
- Shawe-Taylor J, Cristianini N (2004) Kernel methods for pattern analysis. Cambridge University Press, Cambridge
- Tikhonov AN, Arsenin VY (1979) Methods for solving ill-posed problems. Nauka, Moscow
- Vapnik VN (1998) Statistical learning theory. Wiley, New York
- Vovk V (2013) Kernel ridge regression. In: Empirical Inference: Festschrift in Honor of Vladimir N. Vapnik, Springer, Berlin, Heidelberg, pp 105–116
- Wainberg M, Alipanahi B, Frey BJ (2016) Are random forests truly the best classifiers? *J Mach Learn Res* 17(1):3837–3841
- Willmott CJ, Matsuura K (2005) Advantages of the mean absolute error (MAE) over the root mean square error (RMSE) in assessing average model performance. *Clim Res* 30(1):79–82
- Young DM (2003) Iterative solution of large linear systems. Dover Publications, Mineola
- Zheng A, Casari A (2018) Feature engineering for machine learning: principles and techniques for data scientists. O'Reilly Media, Inc, Newton

Publisher's Note Springer Nature remains neutral with regard to jurisdictional claims in published maps and institutional affiliations.